Recibido: 22/12/2021
Aceptado: 22/06/2022

REVISTA DE TELEDETECCIÓN
Asociación Española de Teledetección
(2022) 60, 29-46
ISSN 1133-0953
EISSN 1988-8740
https://doi.org/10.4995/raet.2022.16915

Cover classifications in wetlands using Sentinel-1 data (Band C): a case study in the Parana river delta, Argentina

Mariela Rajngewerc *[1,2], Rafael Grimson [1,2], Juan Lucas Bali [3], Priscilla Minotti [1], Patricia Kandus [1]

[1] *Instituto de Investigación e Ingeniería Ambiental, Universidad Nacional de San Martín, Buenos Aires, Argentina.*
[2] *Consejo Nacional de Investigaciones Científicas y Técnicas (CONICET), Ciudad Autónoma de Buenos Aires, Argentina.*
[3] *YTEC, YPF-CONICET, Buenos Aires, Argentina.*

Abstract: With the launch of the Sentinel-1 mission, for the first time, multitemporal and dual-polarization C-band SAR data with a short revisit time is freely available. How can we use this data to generate accurate vegetation cover maps on a local scale? Our main objective was to assess the use of multitemporal C-Band Sentinel-1 data to generate wetland vegetation maps. We considered a portion of the Lower Delta of the Paraná River wetland (Argentina). Seventy-four images were acquired and 90 datasets were created with them, each one addressing a combination of seasons (spring, autumn, winter, summer, complete set), polarization (VV, HV, both), and texture measures (included or not). For each dataset, a Random Forest classifier was trained. Then, the kappa index values (κ) obtained by the 90 classifications made were compared. Considering the datasets formed by the intensity values, for the winter dates the achieved kappa index values (κ) were higher than 0.8, while all summer datasets achieved κ up to 0.76. Including feature textures based on the GLCM showed improvements in the classifications: for the summer datasets, the κ improvements were between 9% and 22% and for winter datasets improvements were up to 15%. Our results suggest that for the analyzed context, winter is the most informative season. Moreover, for dates associated with high biomass, the textures provide complementary information.

Key words: grey level co-occurrence matrix, synthetic aperture radar, vegetation cover, land cover, classification.

Clasificiación de coberturas en humedales utilizando datos de Sentinel-1 (Banda C): un caso de estudio en el delta del río Paraná, Argentina

Resumen: Con el lanzamiento de la misión Sentinel-1, por primera vez, datos SAR de banda C multitemporales y de polarización dual, con un tiempo de revisión corto, están disponibles de forma gratuita. ¿Cómo podemos utilizar estos datos para generar mapas precisos de cobertura vegetal a escala local? Nuestro principal objetivo fue evaluar el uso de datos multitemporales de banda C Sentinel-1 para generar mapas de vegetación en humedales. Consideramos una porción del humedal del Bajo Delta del Río Paraná (Argentina). Utilizamos setenta y cuatro imágenes y creamos noventa conjuntos de datos distintos con ellas, cada uno abordando una combinación de estaciones (primavera, otoño, invierno, verano, conjunto completo), polarización (VV, HV, ambas) y medidas de textura (incluidas o no). Para cada conjunto de datos, se entrenó un clasificador *Random Forest*. Luego, se compararon los valores de índice kappa (κ) obtenidos por las 90 clasificaciones realizadas. Teniendo en cuenta los conjuntos de datos formados por los valores de intensidad de la señal del radar, para las fechas de invierno los

To cite this article: Rajngewerc, M., Grimson, R., Bali, J.L., Minotti, P., Kandus, P. 2022. Cover classifications in wetlands using Sentinel-1 data (Band C): a case study in the Parana river delta, Argentina. *Revista de Teledetección*, *60*, 29-46. https://doi.org/10.4995/raet.2021.16915

* *Corresponding author: mraj@unsam.edu.ar*

valores κ obtenidos fueron superiores a 0,8, mientras que los conjuntos de datos de verano obtuvieron κ menores a 0,76. La inclusión de los atributos de texturas basados en las matrices de GLCM mostraron mejoras en las clasificaciones: para los conjuntos de datos de verano, las mejoras de κ estuvieron entre un 9% y un 22% y para los de invierno, las mejoras fueron de hasta un 15%. Nuestros resultados sugieren que para el contexto analizado, el invierno es la temporada más informativa. Además, para las fechas asociadas con alta biomasa, las texturas proporcionan información complementaria.

Palabras clave: matriz de co-ocurrencia de nivel de gris, radar de apertura sintética, cobertura vegetal, cobertura terrestre, clasificación.

1. Introduction

The study of wetlands has become increasingly important since they host a large part of the world's biodiversity, play a key role in biogeochemical and hydrological cycles, and provide important social benefits (Millenium Ecosystem Assessment, 2005). Also, these ecosystems are subject to growing pressures mainly due to changes in land use (Lehner and Döll, 2004). Remote sensing is a suitable tool for studying wetlands where getting *in-situ* measurements is difficult and expensive due to their frequently constrained field access (Gallant, 2015). Remote sensing offers a wide range of spatial and temporal scales and is less costly than fieldwork-based research (Brisco et al., 2011; Gallant, 2015). Also, although the acquisition of satellite images can be expensive, since 2014, the ESA Copernicus programme offers free and open satellites from all over the world.

Satellite scenes from Synthetic Aperture Radars (SAR) are being used for wetland characterization and monitoring (Hess et al., 2003; Salvia et al., 2009; Arsen et al., 2013). These images provide information about the geometric and dielectric characteristics of the observed target. Depending on the sensor and target characteristics, the SAR signal can penetrate through the vegetation and provide information about soil, flood conditions, and underneath vegetation (Meyer, 2019). In high biomass wetlands, the radar signal interacts with multiple scatters within the natural medium (volume scatter) resulting in a rise of the cross-polarization backscatter (Martí-Cardona et al., 2010; Tsyganskaya et al., 2018; Meyer, 2019). The scattering mechanisms may change over time according to the vegetation phenology, flooding events, and other environmental conditions (Kandus et al., 2001; Betbeder et al., 2015). Thus, SAR may enable wetlands land-cover classes identification through the temporal change in the backscattering mechanisms (Dabboor and Brisco, 2018; Grimson et al., 2019).

In the last years, access to C-band SAR data has been provided by the European Space Agency due to the launch of the Copernicus Sentinel-1 constellation (Sentinel-1A and Sentinel-1B). SAR imagery are usually expensive mainly due to their active system (it generates its own energy). In contrast, Copernicus programme provides free SAR multitemporal images for all over the world. This mission provides multitemporal and multipolarization (VH, VV) SAR images. Multitemporal C-Band data can enhance wetland classification schemes, by accounting flood changes and vegetation phenology (Salvia et al., 2008; Vanama et al., 2020). However, characterizing vegetation types in high-vegetated wetlands using C-band data has been challenging due to the modest potential of this band to penetrate forest canopies (Sivasankar et al., 2018; Meyer, 2019; Numbisi and Coillie, 2020; Morandeira et al., 2021). In areas where the vegetation is sufficiently dense, backscatter mean values may be similar between different vegetation types.

Image textures are measurements that provide valuable information about the spatial variation of the spectral brightness of a pixel in an image (Hall-Beyer, 2017). Although the land-cover classes may have similar backscatter mean values, they may be identified by their textures (Oliver and Quegan, 2004). One of the most popular methods to calculate texture in remote sensing is based on the Grey Level Co-occurrence Matrix (GLCM) (Haralick, 1979). The GLCM describes the spatial

relationship of image pixel values with their spatial distribution in the landscape by describing the frequency with which different combinations of brightness values occur for each pixel in its predefined neighborhood (Hall-Beyer, 2017). Including GLCM textures measurement derived from SAR images had shown an improvement in vegetation discrimination when using single-date SAR data (Treitz et al., 2000; Arzandeh and Wang, 2002; Krishna et al., 2018; Panuju et al. 2019) or single-polarization SAR data (Kurvonen et al., 1999; Lin et al., 2018). SAR texture measurements may change according to the phenological vegetation state. Thus, multitemporal textures may provide information that improves multitemporal backscatter classifications. The combination of spectral brightness with texture characteristics has great potential for remotely sensed images classifications (Lloyd et al., 2004; Kupidura, 2019; Pulella et al., 2020). Caballero et al. (2020) showed that including multitemporal GLCM textures derived from Sentinel-1 improved the agricultural crops classification in the Bonaerense Valley of the Colorado River (Buenos Aires, Argentina). Also, Numbisi et al. (2019) showed that texture-based maps from multi-season Sentinel-1 imagery for forest classification in Cameroon outperformed the maps obtained using optical imagery.

The performance of remote sensing image classification is determined by the selection and manipulation of remote sensing data, as well as the classification method (Lu and Weng, 2007). A wide range of classifiers have been investigated for land-cover classification using remote sensing data, including Support Vector Machines (Huang et al., 2002), Decision Tree (Otukei and Blaschke, 2010), Neural Networks (Ball et al., 2017), among others. Random Forest (RF) has become one of the most widely used supervised algorithms for wetlands mapping in recent years (Mohammadimanesh et al., 2018; Larocque et al., 2020; Mahdianpari et al., 2020) due to its high accuracy of its classification results, its ability to handle high data dimensionality and multicollinearity, its resistance to overfitting, and its training and prediction procedures are fast (Belgiu and Drăguţ, 2016).

Our aim was to identify the most appropriate set of Sentinel-1B scenes and to study the contribution of C-Band SAR textural data for vegetation cover classification in a densely vegetated wetland. We hypothesized that including textures could be beneficial in this context. We also evaluated if the GLCM textures introduce improvements to the classifications made with one or more polarization, with scenes from one or more seasons of the year. We used as a case of study a section of the Lower Delta of the Paraná River (Argentina) wetland, where the environment is characterized by having phenological and hydrological variability.

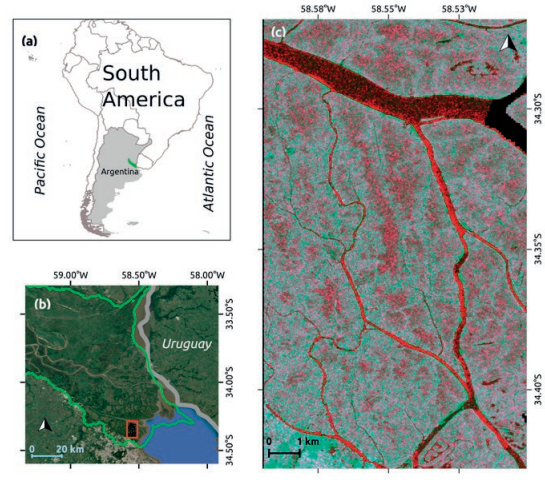

Figure 1. Study area. (a) Location in South America; (b) Location of the study area in the Paraná River Delta; (c) Study area on a representative Sentinel-1 scene subset, date 20th August 2018. The image is a RGB band composition of the Sentinel-1 scene (Red channel = VH/VV ratio; Green channel = VV polarization; Blue channel = VH polarization).

2. Materials

2.1. Case Study: the Lower Delta of the Paraná River

Our case study area was selected because of the existence of a ground-truth database, previous classifications with optical imagery (Kandus et al., 1999), and a wide expert knowledge by two specialists in the vegetation of the studied region. The study area corresponds to a portion of the Lower Delta of the Paraná River wetland, located in Buenos Aires, Argentina (Figure 1), encompassing approximately 100 km^2 (central coordinates: 34.35°S 58.55°W). The climate is

temperate, with a mean annual temperature of 16.7°C, and humid; the annual mean precipitation rounds 1000 mm. The hydrological regime is the result of combined moon tides and wind surges. The tidal amplitude is lower than 1 m. However, tides can reach 3 m above mean sea level during south-east winds (Kandus et al., 2003).

The islands in this region have levees in their perimeter; these result from the accumulation of sediments produced by the Paraná distributary rivers (Kandus et al., 2006). Figure 2 presents a description of the vegetation of the area. Over the natural levees, there are Willow (*Salix* spp.) and Poplar (*Populus* spp.) forest plantations, fruit orchards, and secondary forests (that grow after the abandonment of fruit or forest plantations). Towards the islands' interior, Ceibo forest (*Erythrina crista-galli*) or isolated Ceibos can be found with Cortadera marshes (*Scirpus giganteus*) in the understory. In the islands' centre, where the soil is permanently saturated, Cortadera (*S. giganteus*) is the dominant species. Junco (*Schoenoplectus californicus*) beds are established on the edge of watercourses forming narrow strip marshes (Kandus et al., 2006).

Land cover profile scheme	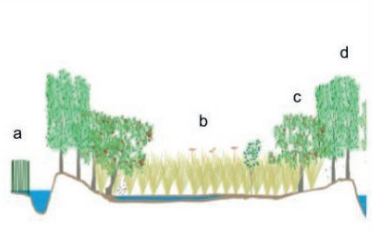			
Reference	a	b	c	d
Class name	Junco marsh	Cortadera marsh	Ceibo Forest	Willow plantation
Dominant Species	*Schoenoplectus californicus*	*Scirpus giganteus*	*Erithina crista-galli*	*Salix* spp.
Description	The Junco plant looks like long, nearly vertical, cylinder shoots.	The cortadera plant is composed of long wide and thick leaves, with nearly uniform vertical density.	The trunk is woody and irregular. The branches have thorns. These plants blossom in October.	Willows have a flexible wood and elongated leaves: The leaves often have serrated edges. These are dioecious plants. The leaves appear between October and November.
Vegetation height (m)	2.5	1.5-2	< 6	< 12
Plant coverage	50-70%	70-90%	40-60%	80%
Plant phenology (deciduous / perennial)	Perennial	Perennial	Deciduous	Deciduous
Soil conditions (permanently flooded, saturated, dry, alternating dry or saturated)	Permanently flooded with strong water circulation	Regularly flooded / Always saturated	Regularly flooded / Always saturated	Occasionally flooded / Partially regulated

Figure 2. Classes description. Land cover types of the Lower Delta of the Paraná River and their main characteristics descriptions (Kandus et al., 1999; Grings et al., 2006; Kandus et al., 2006).

2.2. Remote Sensing Data

2.2.1. SAR Multitemporal Data

Sentinel-1 is a European Spatial Agency mission formed by a constellation of two C-Band (5.405 GHz) SAR satellites: Sentinel-1A and Sentinel-1B. In this study, we used a total of 74 Sentinel-1B images. The acquisitions span from October 2016 to April 2019 with a revisit time of 12 days, except for four missing dates (2017-03-22, 2018-08-08, 2019-02-28, and 2019-03-12). Sentinel-1 scenes were acquired in the Interferometric Wide Swath (IW) mode in VV and VH polarizations. All the acquisitions have near incidence angles of 29.5° and far incidence angles of 45.3°. The scene product type was Level-1 High-Resolution Ground Range Detection (GRD) with a pixel spacing of 10 m × 10 m. The data is available via the Copernicus website (https://scihub.copernicus.eu/dhus/). Scenes were pre-processed within SNAP software using the Sentinel-1 Toolbox (ESA Sentinel Application Platform, 2019).

Pre-processing steps included: thermal noise removal, border noise removal, orbit file application, radiometric calibration, speckle filtering (Refined Lee), terrain flattening, and terrain correction. The refined Lee speckle filter was selected based on its wide use in wetland SAR applications and on its good performance according to a previous assessment (Morandeira, et al., 2016). After processing, the final production was of a geocoded SAR backscattering γ_0 coefficient image for each scene (Filipponi, 2019). Although the topography of the considered study area is extremely flat and does not play a central role, the preference for the γ_0 coefficient was the possibility of adapting the procedure used in this study to areas in which the topography plays a key role.

2.3. Texture Data

One of the most used methods to calculate texture in remote sensing is based on the Grey Level Co-occurrence Matrix (GLCM) (Haralick, 1979; Hall-Beyer, 2017). In this study, GLCM matrices

were generated using a 5×5 window size, in eight directions (the four pixels' neighbours and the four pixels' in the diagonal), and one-pixel displacement. The GLCM texture measures were calculated over the 74 images for both polarizations using the Sentinel-1 Toolbox from SNAP (ESA Sentinel Application Platform, 2019). According to Hall-Beyer (2017), the following texture measurements were computed from the GLCM: Contrast, Entropy, Variance and Correlation.

2.4. Wetland cover types

The Lower Delta of the Paraná River is a densely vegetated wetland and its five major cover classes are Water, Ceibo Forest, Willow Plantation, Cortadera Marsh, and Junco Marsh (Kandus et al., 2006). Considering previous studies in the area (Kandus et al., 2003; Kandus and Malvárez, 2004; Kandus et al., 2006), two high-resolution optical images (Planet Team, 2017), a database of ground-truth data and expert knowledge in the area, a total of 496 Regions of Interest (ROIs) were obtained (between 98 to 100 ROIs, for each class). Each ROI corresponds to a single pixel in the Sentinel-1B stacks.

The backscatter multitemporal series from each vegetation class are presented in Figure 3. The multitemporal GLCM series are presented in Figure 4 and Figure 5.

3. Methods

3.1. Datasets

A total of 90 multitemporal datasets were derived from the 74 Sentinel-1 scenes, by combining the variables and categories described in Table 1. Each dataset was named using the following format: in the first place the selected set of dates was specified (FullYear, Summer, Spring, Autumn, or Winter), in the second place the type of polarizations was specified (XP: cross-polarization, CP: copol, DP: dual polarization) and on the third place the

Table 1. Variables of the 74 Sentinel-1 scenes, determining the 90 datasets assessed. Each dataset in this work is formed by a type of polarization, season and pixel data. This table shows the description of each category.

Variables	Categories	Description
Polarization	DP	VH and VV polarizations
	XP	Cross-polarization (VH) polarization
	CP	Copolarization (VV) polarization
Season	Spring	Images corresponding to the following dates: 2016-10-05 2016-10-17 2016-10-29 2016-11-10 2016-11-22 2016-12-04 2016-12-16 2017-09-30 2017-10-12 2017-10-24 2017-11-05 2017-11-17 2017-11-29 2017-12-11 2018-09-25 2018-10-07 2018-10-19 2018-10-31 2018-11-12 2018-11-24 2018-12-06 2018-12-18
	Summer	Images corresponding to the following dates: 2016-12-28 2017-01-09 2017-01-21 2017-02-02 2017-02-14 2017-02-26 2017-03-10 2017-12-23 2018-01-04 2018-01-16 2018-01-28 2018-02-09 2018-02-21 2018-03-05 2018-03-17 2018-12-30 2019-01-11 2019-01-23 2019-02-04 2019-02-16
	Autumn	Images corresponding to the following dates: 2017-04-03 2017-04-15 2017-04-27 2017-05-09 2017-05-21 2017-06-02 2017-06-14 2018-03-29 2018-04-10 2018-04-22 2018-05-04 2018-05-16 2018-05-28 2018-06-09 2018-06-21 2019-03-24 2019-04-05 2019-04-17 2019-04-29
	Winter	Images corresponding to the following dates: 2017-06-26 2017-07-20 2017-08-01 2017-08-13 2017-08-25 2017-09-06 2017-09-18 2018-07-03 2018-07-15 2018-07-27 2018-08-20 2018-09-01 2018-09-13
	Full Year	Images correspond to all the season's dates.
Pixel data	NoText	The γ_0 backscatter values.
	Contrast	The γ_0 backscatter values and the GLCM-Contrast values.
	Correlation	The γ_0 backscatter values and the GLCM-Correlation values.
	Variance	The γ_0 backscatter values and the GLCM-Variance values.
	AllText	The γ_0 backscatter, the GLCM-Contrast, GLCM-Correlation, GLCM-Entropy and GLCM-Variance values.

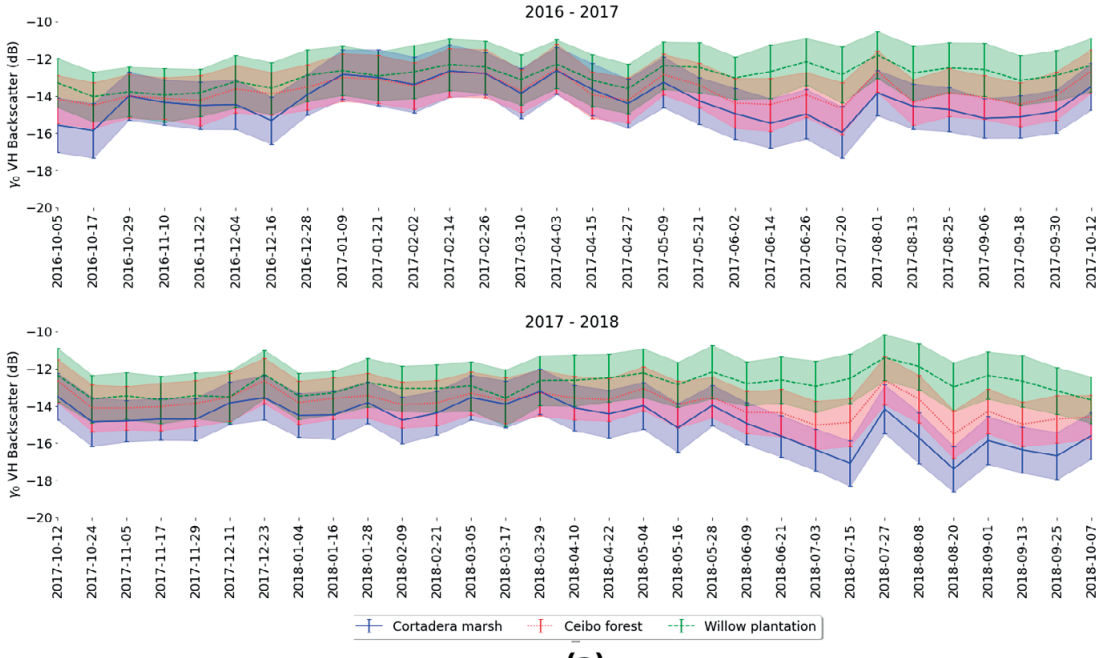

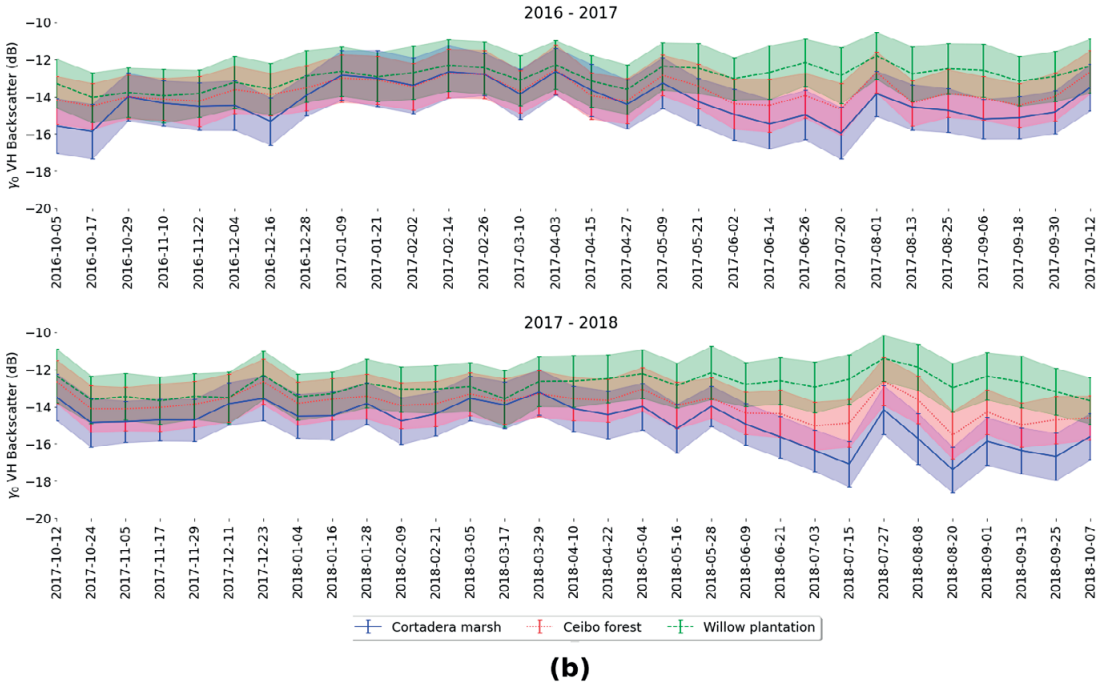

Figure 3. Multitemporal series profiles of Sentinel-1 backscatter values for the dominant vegetation cover classes of the studied portion of the Lower Delta of the Paraná River wetland. The plot shows for each date, the mean backscatter values per class. (a) Shows the VH polarization values; (b) shows the VV polarization values.The background colour is associated with the corresponding dates' season. Green is used for summer dates, lightgreen for spring dates, lightred for autumn dates and red for winter dates.

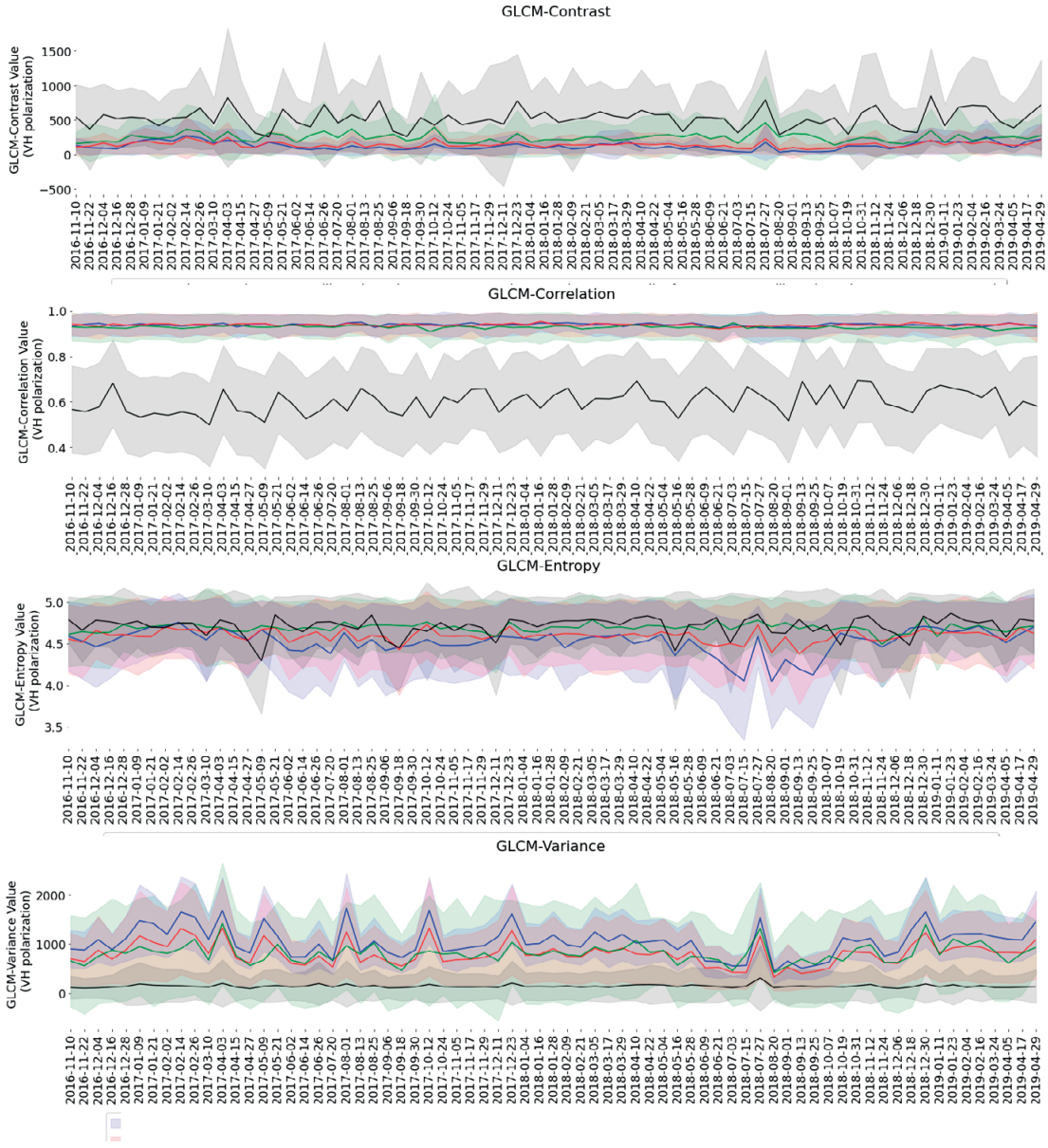

Figure 4. Multitemporal series profiles of the GLCM-Contrast, GLCM-Correlation, GLCM-Entropy and GLCM-Variance values from the vegetation cover classes of the studied area. This Figure shows the values obtained using the VH polarization.

type of textures was specified (NoText, Variance, Entropy, Correlation, Covariace, or AllText). For example: the Summer_XP_NoText dataset corresponds to the one formed by the summer dates of the Cross-polarization Images using the Intensity values without texture measurements; the Summer_XP_Variance corresponds to the dataset formed by the summer dates of the Cross-polarization Images using the Intensity values and the GLCM-Variance texture measurements.

3.2. Classification algorithm

Random forest (RF) algorithm is an ensemble of decision trees (Breiman, 2001) widely used for classification tasks (Pal, 2005; LaRocque et al.,

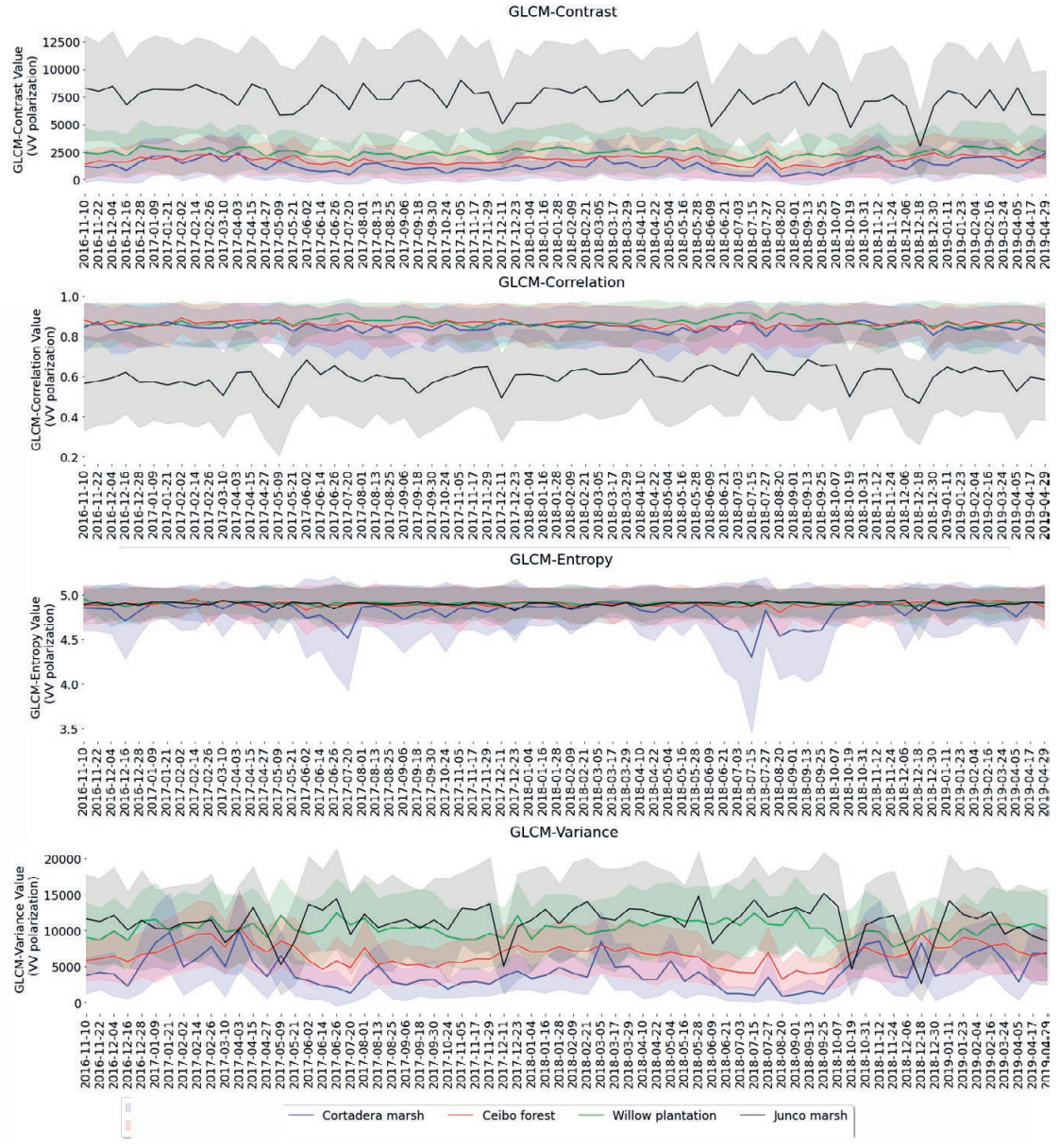

Figure 5. Multitemporal series profiles of the GLCM-Contrast, GLCM-Correlation, GLCM-Entropy and GLCM-Variance values from the vegetation cover classes of the studied area. This Figure shows the values obtained using the VV polarization.

2020). Each tree is formed by a random subset of features and is trained using a random subset of the training samples. The main benefit of these random steps is that this way, the algorithm generates different trees. Therefore, we obtain a decrease in the variance of the forest estimator. Once all the trees are trained, we can predict an input class. First, the algorithm predicts the input class in each tree of the forest and then selects the most repeated class as the RF classifier's predicted class.

In this study, the RF algorithm was applied to all the datasets described in the previous section. The number of trees was adjusted using a cross-validation procedure. RF was carried out using the implementation provided by the scikit-learn (Pedregosa et al., 2011) package in Python 3.6.

3.3. Accuracy Assessments

For each dataset classification, accuracy assessments were performed using a random test set of 200 (40 per class) out of 496 ground truth pixels. The pixels that form the test set correspond to different ROIs than the ones corresponding to the training set. Four measurements were considered for classification evaluations: Overall Accuracy (OA), the Kappa Index value (κ), the user's accuracy (UA), and the producer's accuracy (PA) (Congalton and Green, 2005). First, the comparison between the classifications was evaluated by OA and κ, and then a McNemar statistical test (McNemar, 1947) was applied to study differences between the OA of the classifiers.

4. Results

For each multitemporal dataset, a RF classifier was trained using labeled data from the five-dominant cover classes in the Lower Delta of the Paraná River. The OA and κ of each classification are presented in Table 2.

4.1. Multitemporal analysis of the Intensity datasets

In this section, we will present the results of the Intensity datasets.

4.1.1. Winter and Complete datasets comparisons

The classifications results using the Winter_DP_NoText, Winter_XP_NoText, FullYear_DP_NoText, and FullYear_XP_NoText datasets showed similar κ values, between 0.91-0.94.

In Figures 6 (a), (d), (g), and (j) we can observe that the Intensity-Complete and Intensity-Winter datasets show similar performances for the Ceibo forests, Willow plantations, and Cortadera marshes classes; differences can be observed in the small watercourses where, in the case of FullYear_XP_NoTex and Winter_XP_NoTex, more pixels are classified as Junco marsh class.

In the case of the VH polarization, the PA (Figures 7) values from the Complete dataset were 2.5% higher than the Winter dataset for the Cortadera

Table 2. Classification results. From 74 Sentinel-1 images, 90 datasets were created, each one addressing a combination of seasons (spring, autumn, winter, summer, complete set), polarization (VV, HV, both), and texture measures (included or not). For each dataset, a Random Forest (RF) classifier was trained. This table shows, for each dataset, the overall accuracy (OA) and Kappa Index value (κ) values obtained by the corresponding RF classifier.

		Intensity		Intensity + All textures		Intensity + GLCM Contrast		Intensity + GLCM Correlation		Intensity + GLCM Entropy		Intensity + GLCM Variance	
Polarization	Season	κ	OA (%)	κ	OA (%)	κ	OA (%)	κ	OA (%)	κ	OA (%)	κ	OA (%)
DUAL (VH, VV)	Full Year	0.94	95.50	0.96	97.00	0.95	96.00	0.94	95.00	0.94	95.00	0.96	96.50
	Spring	0.80	84.00	0.92	94.00	0.85	88.00	0.83	86.50	0.84	87.50	0.96	97.00
	Summer	0.76	80.50	0.90	92.00	0.78	82.50	0.76	80.50	0.79	83.00	0.90	92.00
	Autumn	0.90	92.00	0.91	93.00	0.89	91.00	0.89	91.50	0.89	91.50	0.93	94.50
	Winter	0.94	95.50	0.96	97.00	0.96	96.50	0.96	96.50	0.94	95.50	0.96	97.00
VH	Full Year	0.94	95.50	0.97	97.50	0.95	96.00	0.94	95.50	0.93	94.00	0.97	97.50
	Spring	0.80	84.00	0.91	93.00	0.79	83.00	0.78	82.50	0.81	84.50	0.91	93.00
	Summer	0.70	76.00	0.84	87.50	0.74	79.50	0.71	77.00	0.71	76.50	0.78	82.50
	Autumn	0.82	85.50	0.88	90.50	0.82	85.50	0.78	82.50	0.81	85.00	0.89	91.00
	Winter	0.91	93.00	0.94	95.00	0.91	94.00	0.92	93.50	0.91	92.50	0.95	96.00
VV	Full Year	0.87	89.50	0.94	95.50	0.89	91.00	0.91	92.50	0.87	89.50	0.92	93.50
	Spring	0.76	81.00	0.88	90.50	0.81	84.50	0.79	83.50	0.77	81.50	0.84	87.50
	Summer	0.68	74.00	0.83	86.00	0.74	79.00	0.68	74.50	0.65	72.00	0.76	81.00
	Autumn	0.78	82.50	0.89	91.50	0.82	85.50	0.84	87.00	0.77	81.50	0.84	87.50
	Winter	0.80	84.00	0.92	93.50	0.88	90.50	0.89	91.50	0.79	83.50	0.84	87.50

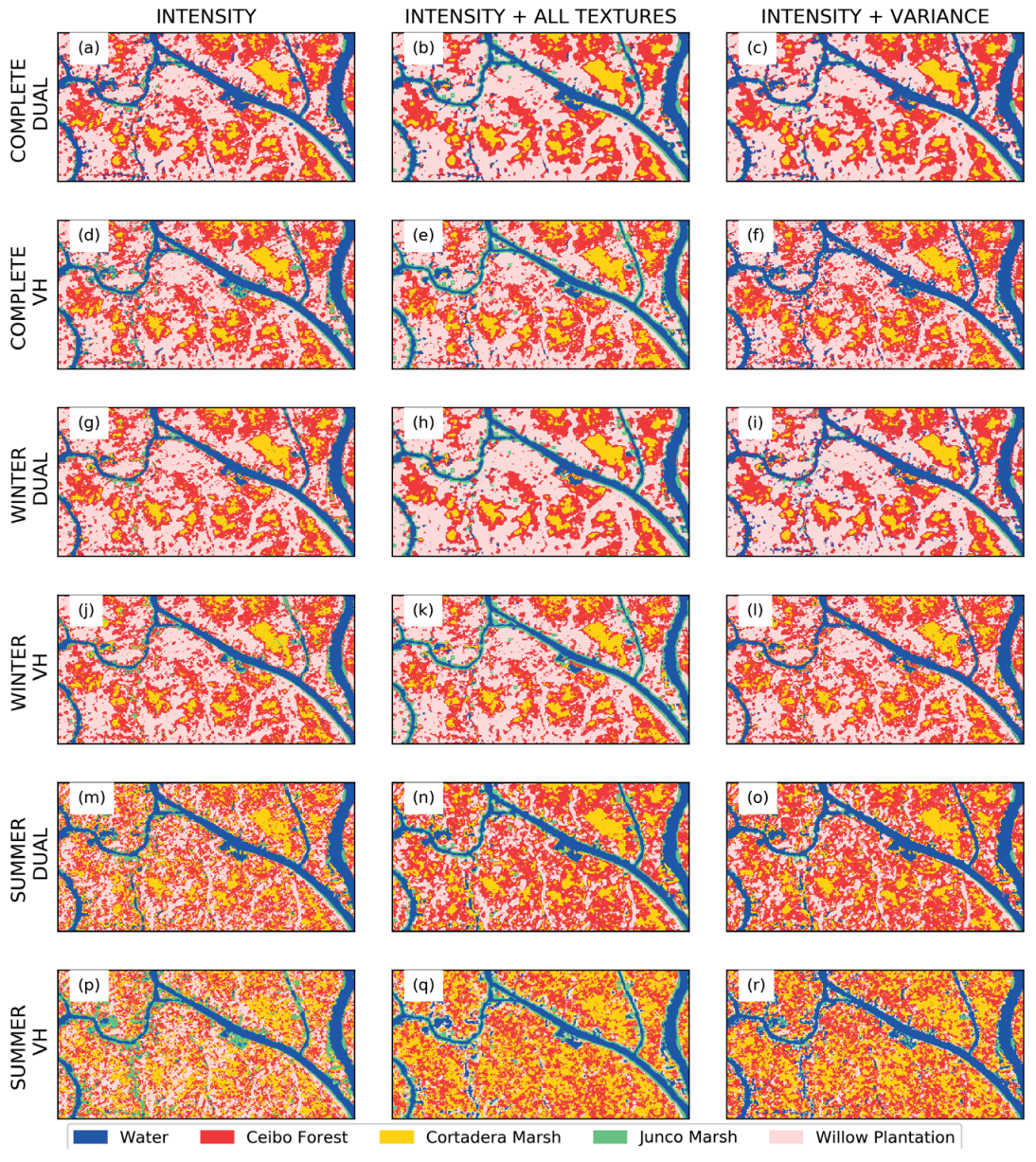

Figure 6. Classification results of the Random Forest algorithm. The figure shows the obtained classifications applied over the lower part of the study area correspondig to the following datasets: (a) FullYear_DP_NoTex; (b) FullYear_DP_AllTex; (c) FullYear_DP_Variance; (d) FullYear_XP_NoTex; (e) FullYear_XP_AllText; (f) FullYear_XP_Variance; (g) Winter_DP_NoTex; (h) Winter_DP_AllTex;(i) Winter_DP_Variance; (j) Winter_XP_NoTex; (k) Winter_XP_AllTex; (l) Winter_XP_Variance; (m) Summer_DP_NoTex; (n) Summer_DP_AllTex; (o) Summer_DP_Variance; (p) Summer_XP_NoTex (q) Summer_XP_AllTex; (r) Summer_XP_Variance.

marsh and Junco marsh classes. In the case of the Willow Plantation class the PA corresponding to the Complete dataset was 7.5% higher than the one corresponding to the Winter dataset.

In the case of the Dual polarization, Complete and Winter datasets showed very similar PA and UA values (Figures 7 and 8). The highest difference was observed for the Ceibo Forest class, the

Table 3. McNemar test for Winter dataset. The McNemar statistical test was used to study the difference between the Overall Accuracy values of the classifications obtained with different datasets. The null hypothesis is that the two compared model's performances are equal. The McNemar test will reject this null hypothesis if the p-value is less than 0.05 (considering a 95% confidence level).

Dataset	Dataset	p-value
Summer_DP_NoTex	Winter_XP_NoTex	1.20×10^{-4}
	Winter_DP_NoTex	3.00×10^{-7}
	FullYear_XP_NoTex	2.60×10^{-6}
	FullYear_CP_NoTex	2.70×10^{-3}
	FullYear_DP_NoTex	6.60×10^{-7}
Summer_XP_NoTex	Winter_XP_NoTex	3.50×10^{-7}
	Winter_CP_NoTex	4.10×10^{-2}
	Winter_DP_NoTex	6.80×10^{-9}
	FullYear_XP_NoTex	1.50×10^{-8}
	FullYear_CP_NoTex	7.34×10^{-5}
	FullYear_DP_NoTex	1.50×10^{-8}
Summer_CP_NoTex	Winter_XP_NoTex	4.80×10^{-7}
	Winter_CP_NoTex	2.70×10^{-3}
	Winter_DP_NoTex	9.00×10^{-10}
	FullYear_XP_NoTex	4.10×10^{-9}
	FullYear_CP_NoTex	2.80×10^{-6}
	FullYear_DP_NoTex	9.00×10^{-10}

Table 4. McNemar test for Summer datasets. The McNemar statistical test was used to study the difference between the Overall Accuracy values of the classifications obtained with different datasets. The null hypothesis is that the two compared model's performances are equal. The McNemar test will reject this null hypothesis if the p-value is less than 0.05 (considering a 95% confidence level).

Dataset	Dataset	p-value
Winter_DP_NoTex	Spring_XP_NoTex	1.3×10^{-4}
	Spring_CP_NoTexI	2.2×10^{-6}
	Spring_DP_NoTex	2.3×10^{-5}
	Summer_XP_NoTex	6.9×10^{-9}
	Summer_CP_NoTex	9.0×10^{-10}
	Summer_DP_NoTex	3.0×10^{-7}
	Autumn_XP_NoTex	3.3×10^{-4}
	Autumn_CP_NoTex	2.3×10^{-6}
	Winter_CP_NoTex	2.3×10^{-5}
Winter_XP_NoTex	Spring_XP_NoTex	2.7×10^{-3}
	Spring_CP_NoTex	1.9×10^{-4}
	Spring_DP_NoTex	8.6×10^{-4}
	Summer_XP_NoTex	3.5×10^{-7}
	Summer_CP_NoTex	4.8×10^{-7}
	Summer_DP_NoTex	1.2×10^{-4}
	Autumn_XP_NoTex	1.4×10^{-2}
	Autumn_CP_NoTex	2.0×10^{-4}
	Winter_CP_NoTex	1.3×10^{-3}

Winter_DP_NoTex dataset had a PA of 92.5% whereas the FullYear_DP_NoTex resulted in 87.5%.

4.1.2. Season datasets comparisons

For each polarization, in the Intensity datasets, we observed that the Winter dates achieved higher κ values than using Summer, Spring, and Autumn datasets. Furthermore, the Winter_DP_NoTex dataset got a κ values 15% higher than the Summer_DP_NoTex, Summer_XP_NoTex, Summer_CP_NoTex, Spring_DP_NoTex, Spring_XP_NoTex, Spring_CP_NoTex, Autumn_XP_NoTex, Autumn_CP_NoTex, and Winter_CP_NoTex datasets. The McNemar test confirmed a statistical difference between the classification obtained using the Winter_DP_NoTex dataset and the ones obtained with each of the aforementioned datasets (Table 3).

Figures 6 (m) and (p) show the classification results obtained using the Summer dataset where we can observe a noisy pattern. The Summer_DP_NoTex, Summer_XP_NoTex, and Summer_CP_NoTex datasets got κ values between 0.68 and 0.76, resulting in the lowest achieved for the Intensity datasets.

The Summer_DP_NoTex, Summer_XP_NoTex, and Summer_CP_NoTex PA values (Figure 7) from the Ceibo, Willow Plantation, and Junco Marsh classes, were lower than the ones obtained in the Winter, Complete, and Autumn datasets. The Summer_DP_NoTex, Summer_XP_NoTex, and Summer_CP_NoTex showed PA and UA values lower than 70% either for the Ceibo Forest and for the Willow Plantation classes (Figures 7 and 8).

Moreover, when we compared a classification using an Summer_DP_NoTex, Summer_XP_NoTex, and Summer_CP_NoTex dataset with classifications obtained using only Winter_XP_NoTex, Winter_DP_NoTex, FullYear_DP_NoTex, and FullYear_XP_NoTex datasets, the McNemar test reveals that the classifications have a statistical significance difference (Table 4).

4.2. Texture analysis

We compared the performance of the Intensity datasets with the ones that combine Intensity and GLCM-textures.

The datasets that combine Intensity with All-Textures or Variance achieved κ values higher than the Intensity datasets in all the polarisation and seasons (Table 2). In general, the datasets formed by the combination of Intensity with All-Textures or Intensity with Variance values achieved higher κ values than the datasets formed by the combination of Intensity with Entropy, Correlation, or Contrast values. The only exception was in the Winter_CP case.

The FullYear_DP_AllTex, FullYear_XP_AllTex, FullYear_XP_Variance, Winter_DP_AllTex, Spring_DP_Variance, datasets achieved the highest κ values (0.96) and OA (97%) values (Figure 6). The Winter_CP_AllTex and the FullYear_CP_AllTex, datasets achieved κ values lower than the ones corresponding to the VH and Dual polarizations.

For the Summer_DP_NoTex dataset, the κ value was 0.76, an 18% improvement was achieved using the Summer_DP_AllTex datasets or the using the Summer_DP_Variance dataset (Figures 6 (m), (n) and (o)). In the case of the Winter datasets in the Dual polarization, the κ difference between using the datasets that include any of the GLCM textures and the ones that do not were up to 2.2% (Figure 6).

We observed that the Spring_DP_NoTex, Spring_XP_NoTex, Spring_CP_NoTex, Summer_DP_NoTex, Summer_XP_NoTex, and Summer_CP_

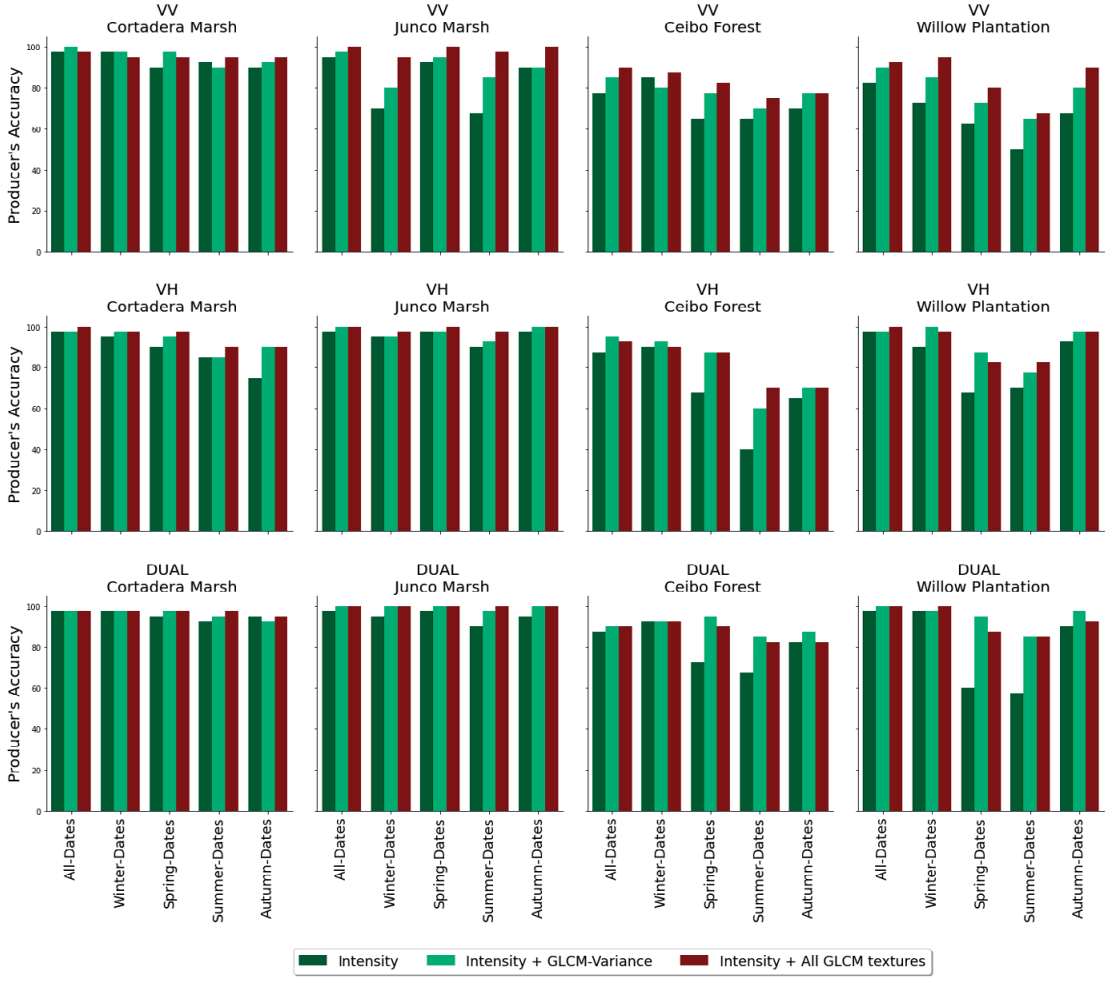

Figure 7. Producer's Accuracies percentage of the Intensity, Intensity+GLCM-Variance and Intensity +GLCM-All Textures datasets.

NoTex datasets registered κ values between 0.68 and 0.80. In these cases, using the All-Textures and Variance dataset showed an improvement between 9 to 22.1% in the κ values. On the other hand, the FullYear_XP_NoTex, FullYear_DP_NoTex, Winter_XP_NoTex, and Winter_DP_NoTex, datasets reported κ between 0.91 and 0.94. In these cases, using the All-Textures and Variance datasets showed less than a 4.4% improvement.

In the case of the Summer and Spring datasets, the incorporation of texture measurements showed an improvement in the PA and UA values for the vegetation classes, in particular for the Ceibo Forest and Willow plantation classes (Figures 7 and 8). The PA corresponding to the Willow Plantation class was 60% for the Spring_DP_NoTex, whereas for the Spring_DP_variance was 95%. In the case of the Ceibo Forest, the PA obtained in the Spring_DP_NoTex and Spring_DP_Variance datasets reached 72.5%, and 95%, respectively.

The PA corresponding to the Willow Plantation class was 57.5% for the Summer_DP_NoTex, whereas for the Summer_DP_AllTex and Summer_DP_Variance was 85%. In the case of the Ceibo Forest, the PA obtained in the Summer_DP_NoTex and Summer_DP_Variance datasets, reached 67.5%, and an 85%, respectively.

The All-Textures dataset identifies the water next to the land as junco marshes, while the Variance dataset does not show this effect (Figure 6).

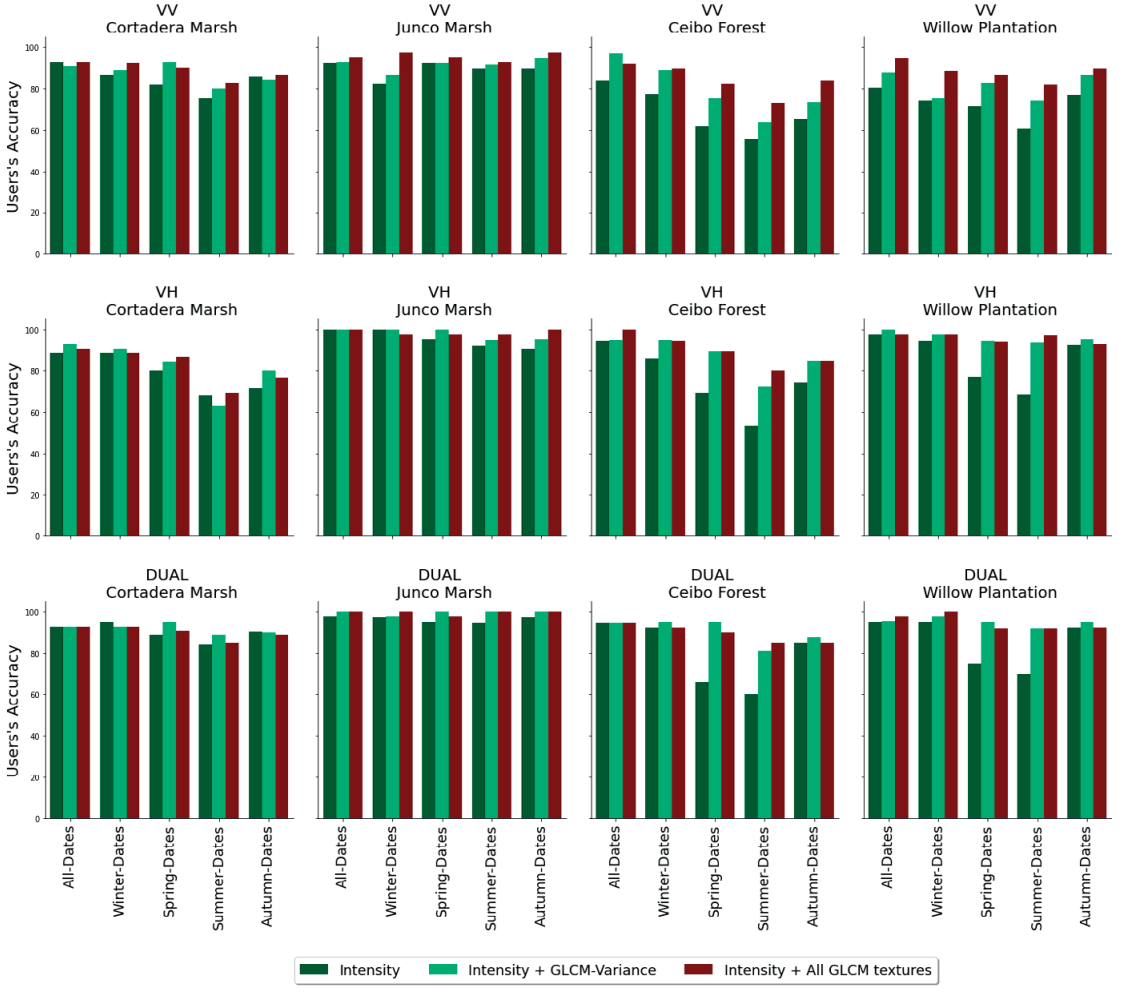

Figure 8. User's Accuracies percentage of the Intensity, Intensity+GLCM-Variance and Intensity +GLCM-All Textures datasets.

5. Discussion

The general objective of this work was to study the potential of Sentinel-1 multitemporal imagery for the generation of an accurate vegetation cover map of the Lower Delta of the Paraná River wetland at a local scale. Specifically, we analyzed how the data from different seasons and the incorporation of GLCM textures influence the classification accuracies. The use of SAR multitemporal data provides valuable insights for wetlands vegetation cover classification (Ozesmi and Bauer, 2002). Using multiple images from the same region can improve the reliability of the generated maps (Tsyganskaya et al., 2018). However, the selection of dates constitutes a decisive factor to achieve proper classification accuracies. We found that the classification performance values obtained for the Winter dataset were as high as those obtained using the Complete series, in the case of the VH and Dual polarizations. Classifications obtained for the Summer datasets showed low κ, OA, PA, and UA values. Moreover, noisy patterns can be observed in the complete scene classification with these datasets (Figure 6). Concerning the combination of SAR and GLCM texture data, Mishra et al. (2019) demonstrated the significance of textural features in improving the classification accuracy of heterogeneous landscapes. In line with these results, we observed that including multitemporal texture measurements in the intensity datasets improved the performance of the classifications.

The lower classifications performances achieved with the Summer datasets could be associated with the high vegetation biomass during this season. During the summer, an increase in the VH polarization values of the Ceibo Forest class is observed, probably due to the phenological changes in the vegetation. The Willow Plantation and Ceibo Forest classes show similar intensity values on summer dates; both classes have grown leaves, so volume becomes the dominant scattering mechanism (Meyer, 2019). At C-band, most scattering comes from the canopy, having little to no penetration to the ground surface or above-ground vegetation (Bourgeau-Chavez et al., 2015). Therefore, all vegetation classes have high and similar VH values; Figure 3 shows that the backscatter mean values of the Ceibo forest, Willow plantation, and Cortadera Marsh classes are very close during the summer dates compared to what happens in other seasons, especially in 2018.

Winter datasets showed performances comparable to the ones obtained using the Complete series dataset. Forest classes, which have similar mean backscatter values during the summer dates, show differences during the winter dates (Figure 3). Ceibo and Willow are forest classes that have some differences in their distribution in the landscape: the Ceibo class is characterized by being an open forest with a high amount of biomass underneath, whereas the Willow class is characterized by being a closed forest (Kandus et al., 2006). Mueller et al. (2021) showed a backscattered signal difference between forest patches with a dense vegetation density in the understory and those with a low vegetation density in Thuringia (Germany). In line with this study, a possible explanation is that in the case of the Ceibo forest during the winter the microwave radiation may be interacting with the stems, trunks, and, also, with the vegetation underneath, contrary to what may be happening in the Willow class. These differences in the interactions may be the key to distinguish between the Ceibo Forest and the Willow Plantation classes in the Winter datasets.

Tsyganskaya et al. (2018) highlight the importance of using SAR images from different seasons in wetland monitoring, however, in wetlands like the Lower Delta of the Paraná River using winter dates to generate vegetation cover maps seems to be promising. Our results suggest that winter dates seem to be important to incorporate them for vegetation cover classification in the Lower Delta of the Paraná River wetland. In line with the Curse of dimensionality (James et al., 2021), instead of using the total Complete multitemporal data, just using the winter dates is suggest. Moreover, this date selection decrease by around 25% of the amount of information to incorporate in the classification, so, less memory and processing time is needed.

Previous studies have shown that the incorporation of SAR textures improves the accuracy of the coverage maps (Numbisi et al., 2018; Caballero et al., 2020). Our results also demonstrate that incorporating GLCM textures outperforms classifications obtained using just the intensity values in the Lower Delta of the Paraná River.

Although using the datasets formed by the combination of Intensity and GLCM textures showed equal or higher performances than the Intensity datasets, in the case of the Summer and Spring datasets the performance increased more than 9%. As mentioned before, during the summer and the spring the vegetation is dense in the study area, the volume seems to be the main scattering mechanism and backscatter values are very similar between vegetation classes. Hence, the information needed to differentiate between classes may be stored in the image's texture due to the differences in the distribution patterns of each vegetation class in the landscape.

Regarding the choice of the GLCM texture measurement, we found that All-textures and Variance got the highest results. All the studied vegetation classes show the same or even higher PA and UA values for the datasets formed by the combination of Intensity and GLCM textures compared to the ones formed only with Intensity values. The GLCM-Variance deals with the dispersion around the mean of combinations of reference and neighbor pixels in a selected window. As All-textures are formed by 4 textures and Variance by one, following The Curse of dimensionality (James et al., 2021), the Variance datasets could be preferred in future works.

In Figure 6 we can observe that the All-Textures dataset identifies the water next to the land as junco marshes, while the Variance dataset does not show this effect. As Junco marshes are small homogenous zones bordering watercourses, selecting a large window size may introduce spurious transitions between neighboring land cover classes (Gong et al., 1992; Nyoungui et al., 2002). Future experiments will analyze different window sizes for the GLCM textures generation in this study area.

6. Conclusions

While C-band is not usually recommended for coverage mapping in densely vegetated wetlands due to its limited capacity of penetration through vegetation, multitemporal C-band SAR datasets showed high Overall Accuracy and κ performance in the Lower Delta of the Paraná River. The combination of the intensity values and the GLCM textures showed improvements for all the studied multitemporal datasets. It is worth mentioning that even in summer dates, when the vegetation was grown and the intensity mean values between vegetation classes were very similar, including GLCM-Variance or GLCM-(All-textures) textures showed up to 22% of improvement. We suggest including multitemporal GLCM textures in future works since it seems to improve the performance of the classification, and is a fast and simple to compute feature. Regarding the dates selection, using winter dates (or incorporating these dates in the dataset) showed the highest accuracies, and summer datasets had the lowest ones. The winter dates selection and the inclusion of GLCM textures seem to be the key to improve vegetation cover classifications in densely vegetated areas.

References

Arsen, A., Crétaux, J.F., Berge-Nguyen, M., del Rio, R.A. 2013. Remote Sensing-Derived Bathymetry of Lake Poopó. *Remote Sensing, 6*(1),407–420. https://doi.org/10.3390/rs6010407

Arzandeh, S., Wang, J. 2002. Texture Evaluation of RADARSAT Imagery for Wetland Mapping. *Canadian Journal of Remote Sensing, 28*(5), 653–66. https://doi.org/10.5589/m02-061

Ball, J.E., Anderson, D.T., Chan, C.S. 2017. Comprehensive Survey of Deep Learning in Remote Sensing: Theories, Tools, and Challenges for the Community. *Journal of Applied Remote Sensing, 11*(4), 1–54. https://doi.org/10.1117/1.JRS.11.042609

Belgiu, M., Drăguţ, L. 2016. Random Forest in Remote Sensing: A Review of Applications and Future Directions. *ISPRS Journal of Photogrammetry and Remote Sensing, 114*, 24–31. https://doi.org/10.1016/j.isprsjprs.2016.01.011

Betbeder, J., Rapinel, S., Corgne, S., Pottier, E., Hubert-Moy, L. 2015. TerraSAR-X Dual-Pol Time-Series for Mapping of Wetland Vegetation. *ISPRS Journal of Photogrammetry and Remote Sensing, 107*, 90-98. https://doi.org/10.1016/j.isprsjprs.2015.05.001

Bourgeau-Chavez, L., Endres, S., Battaglia, M., Miller, M.E., Banda, E., Laubach, Z., Phyllis Higman, Chow-Fraser, P., Marcaccio, J. 2015. Development of a Bi-National Great Lakes Coastal Wetland and Land Use Map Using Three-Season PALSAR and Landsat Imagery. *Remote Sensing, 7*(7), 8655–8682. https://doi.org/10.3390/rs70708655

Breiman, L. 2001. Random Forests. *Machine Learning, 45*, 5–32. https://doi.org/10.1023/A:1010933404324

Brisco, B., Kapfer, M., Hirose, T., Tedford, B., Liu, J., 2011. Evaluation of C-Band Polarization Diversity and Polarimetry for Wetland Mapping. *Canadian Journal of Remote Sensing, 37*(1), 82–92. https://doi.org/10.5589/m11-017

Caballero, G.R., Platzeck, G., Pezzola, A., Casella, A., Winschel, C., Silva, S.S., Ludueña, E., Pasqualotto, N., Delegido, J. 2020. Assessment of Multi-Date Sentinel-1 Polarizations and GLCM Texture Features Capacity for Onion and Sunflower Classification in an Irrigated Valley: An Object Level Approach. *Agronomy, 10*(6), 845. https://doi.org/10.3390/agronomy10060845

Congalton, R.G., Green, K. 2005. *Assessing the Accuracy of Remotely Sensed Data Principles and Practices*. Florida: Taylor & Francis.

Dabboor, M., Brisco, B. 2018. Wetland Monitoring and Mapping Using Synthetic Aperture Radar, Wetlands Management. *Assessing Risk and Sustainable Solutions*. IntechOpen. https://doi.org/10.5772/intechopen.80224

ESA Sentinel Application Platform. 2019. SNAP. *Version 6.* http://step.esa.int.

Filipponi, F. 2019. Sentinel-1 GRD Preprocessing Workflow. *Proceedings, 18*(1), 11. https://doi.org/10.3390/ECRS-3-06201

Gallant, A.L. 2015. The Challenges of Remote Monitoring of Wetlands. *Remote Sensing, 7*(8), 10938–10950. https://doi.org/10.3390/rs70810938

Gong, P., Marceau, D.J., Howarth, P.J. 1992. *A Comparison of Spatial Feature Extraction Algorithms for Land-Use Classification with SPOT HRV Data, 40*(2), 137-151. https://doi.org/10.1016/0034-4257(92)90011-8

Grimson, R., Morandeira, N.S., Gayol, M.P., Kandus, P. 2019. Freshwater Marsh Classification in the Lower Paraná River Floodplain: An Object-Based Approach on Multitemporal X-Band COSMO-SkyMed Data. *Journal of Applied Remote Sensing, 13*(1), 1–14. https://doi.org/10.1117/1.JRS.13.014531

Grings, F.M., Ferrazzoli, P., Jacobo-Berlles, J.C., Karszenbaum, H., Tiffenberg, J., Pratolongo, P., Kandus, P. 2006. Monitoring Flood Condition in Marshes Using EM Models and Envisat ASAR Observations. *IEEE Transactions on Geoscience and Remote Sensing, 44*(4), 936–942. https://doi.org/10.1109/TGRS.2005.863482

Hall-Beyer, M. 2017. Practical Guidelines for Choosing GLCM Textures to Use in Landscape Classification Tasks over a Range of Moderate Spatial Scales. *International Journal of Remote Sensing, 38*(5), 1312–1338. https://doi.org/10.1080/01431161.2016.1278314

Haralick, R.M. 1979. Statistical and Structural Approaches to Texture. *Proceedings of the IEEE, 67*(5), 786–804. https://doi.org/10.1109/PROC.1979.11328

Hess, L.L., Melack, J.M., Novo, E.M.L.M., Barbosa, C.C.F., Gastil, M. 2003. Dual-Season Mapping of Wetland Inundation and Vegetation for the Central Amazon Basin. *Remote Sensing of Environment, 87*(4), 404–428. https://doi.org/10.1016/j.rse.2003.04.001

Huang, C., L.S.D., Townshend, J.R.G. 2002. An Assessment of Support Vector Machines for Land Cover Classification. *International Journal of Remote Sensing, 23*(4), 725–749. https://doi.org/10.1080/01431160110040323

James, G., Witten, D., Hastie, T., Tibshirani, R. 2021. *An Introduction to Statistical Learning with Applications in R Second Edition*. New York: Springer. https://doi.org/10.1007/978-1-0716-1418-1

Kandus, P., Malvárez, A.I. 2004. Vegetation Patterns and Change Analysis in the Lower Delta Islands of the Paraná River (Argentina). *Wetlands, 24*(3), 620–632. https://doi.org/10.1672/0277-5212(2004)024[0620:VPACAI]2.0.CO;2

Kandus, P., Karszenbaum, H., Frulla, L. 1999. Land Cover Classification System for the Lower Delta of the Paraná River (Argentina): Its Relationship with Landsat Thematic Mapper Spectral Classes. *Journal of Coastal Research, 15*(4), 909–926.

Kandus, P., Karszenbaum, H., Pultz, T., Parmuchi, G., Bava, J. 2001. Influence of Flood Conditions and Vegetation Status on the Radar Backscatter of Wetland Ecosystems. *Canadian Journal of Remote Sensing, 27*, 651–662. https://doi.org/10.1080/07038992.2001.10854907

Kandus, P., Malvárez, A.I., Madanes, N. 2003. Estudio de Las Comunidades de Plantas Herbáceas de Las Islas Bonaerenses Del Bajo Delta Del Río Paraná (Argentina). *Darwiniana,* 41(1–4), 1–16.

Kandus, P., Quintana, R.D., Bó, R.F. 2006. *Patrones de Paisaje y Biodiversidad Del Bajo Delta Del Río Paraná. Mapa de Ambientes*. Buenos Aires: Wetlands International.

Krishna, G.B., Mittal, V. 2018. Land Cover Classification of Full Polarimetric PALSAR Images using Decision Tree based on Intensity and Texture Statistical Features. *International Conference on Recent Innovations in Electrical, Electronics & Communication Engineering (ICRIEECE),* 2018, pp. 739-744. https://doi.org/10.1109/ICRIEECE44171.2018.9009289

Kupidura, P. 2019. The Comparison of Different Methods of Texture Analysis for Their Efficacy for Land Use Classification in Satellite Imagery. *Remote Sensing, 11*(10), 1233. https://doi.org/10.3390/rs11101233

Kurvonen, L., Pulliainen, J., Hallikainen, M. 1999. Retrieval of Biomass in Boreal Forests from Multitemporal ERS-1 and JERS-1 SAR Images. *IEEE Transactions on Geoscience and Remote Sensing, 37*(1), 198–205. https://doi.org/10.1109/36.739154

Larocque, A., Leblon, B., Woodward, R., Bourgeau-Chavez, L. 2020. Wetland Mapping in New Brunswick, Canada with Landsat5-Tm, Alos-Palsar, and Radarsat-2 Imagery. *ISPRS Annals of the Photogrammetry, Remote Sensing and Spatial Information Sciences, 5*, 301–308. https://doi.org/10.5194/isprs-annals-V-3-2020-301-2020

LaRocque, A., Phiri, C., Leblon, B., Pirotti, F., Connor, K., Hanson, A. 2020. Wetland Mapping with Landsat 8 OLI, Sentinel-1, ALOS-1 PALSAR, and LiDAR Data in Southern New Brunswick, Canada. *Remote Sensing, 12*(13), 2095. https://doi.org/10.3390/rs12132095

Lehner, B., Döll, P. 2004. Development and Validation of a Global Database of Lakes, Reservoirs and Wetlands. *Journal of Hydrology, 296*(1–4), 1–22. https://doi.org/10.1016/j.jhydrol.2004.03.028

Lin K-F, Perissin D. 2018. Single-Polarized SAR Classification Based on a Multi-Temporal Image Stack. *Remote Sensing, 10*(7), 1087. https://doi.org/10.3390/rs10071087

Lloyd, C.D., Berberoglu, S., Curran, P.J., Atkinson, P.M. 2004. A Comparison of Texture Measures for the Per-Field Classification of Mediterranean Land Cover. *International Journal of Remote Sensing, 25*(19), 3943–3965. https://doi.org/10.1080/0143116042000192321

Lu, D., Weng, Q. 2007. A Survey of Image Classification Methods and Techniques for Improving Classification Performance. *International Journal of Remote Sensing, 28*(5), 823–870. https://doi.org/10.1080/01431160600746456

Mahdianpari, M., Salehi, B., Mohammadimanesh, F., Brisco, B., Homayouni, S., Gill, E., DeLancey, E.R, Bourgeau-Chavez, L. 2020. Big Data for a Big Country: The First Generation of Canadian Wetland Inventory Map at a Spatial Resolution of 10-m Using Sentinel-1 and Sentinel-2 Data on the Google Earth Engine Cloud Computing Platform. *Canadian Journal of Remote Sensing, 46*(1), 15–33. https://doi.org/10.1080/07038992.2019.1711366

Martí-Cardona, B., López-Martínez, C., Dolz-Ripollés, J., Bladè-Castellet, E. 2010. ASAR Polarimetric, Multi-Incidence Angle and Multitemporal Characterization of Doñana Wetlands for Flood Extent Monitoring. *Remote Sensing of Environment, 114*(11), 2802–2815. https://doi.org/10.1016/j.rse.2010.06.015

McNemar, Q. 1947. Note on the Sampling Error of the Difference between Correlated Proportions or Percentages. *Psychometrika, 12*(2), 153-157. https://doi.org/10.1007/BF02295996

Meyer, F.J. 2019. Spaceborne Synthetic Aperture Radar: Principles, Data Access, and Basic Processing Techniques. in *SAR Handbook: Comprehensive Methodologies for Forest Monitoring and Biomass Estimation*. NASA.

Mishra, V.N., Prasad, R., Rai, P.K., Vishwakarma, A.K., Arora, A. 2019. Performance Evaluation of Textural Features in Improving Land Use/Land Cover Classification Accuracy of Heterogeneous Landscape Using Multi-Sensor Remote Sensing Data. *Earth Science Informatics, 12*(1), 71–86. https://doi.org/10.1007/s12145-018-0369-z

Mohammadimanesh, F., Salehi, B., Mahdianpari, M., Brisco, B., Motagh, M. 2018. Multi-Temporal, Multi-Frequency, and Multi-Polarization Coherence and SAR Backscatter Analysis of Wetlands. *ISPRS Journal of Photogrammetry and Remote Sensing, 142*, 78–93. https://doi.org/10.1016/j.isprsjprs.2018.05.009

Morandeira, N.S., Grimson, R., Kandus, P. 2016. Assessment of SAR speckle filters in the context of object-based image analysis. *Remote Sensing Letters*, *7*(2), 150–159. https://doi.org/10.1080/2150704X.2015.1117153

Morandeira, N.S., Barber, M.E., Grings, F.M., Ahern, F., Kandus, P., Brisco, B. 2021. Response of Multi-Incidence Angle Polarimetric RADARSAT-2 Data to Herbaceous Vegetation Features in the Lower Paraná River Floodplain, Argentina. *Remote Sensing, 13*(13), 2518. https://doi.org/10.3390/rs13132518

Mueller, M.M., Dubois, C., Jagdhuber, T., Pathe, C., Schmullius, C. 2021. Investigation of Sentinel-1 time series for sensitivity to fern vegetation in an european temperate forest. *The International Archives of the Photogrammetry, Remote Sensing and Spatial Information Sciences* XLIII-B3-2021, 127–134. https://doi.org/10.5194/isprs-archives-XLIII-B3-2021-127-2021

Numbisi, F.N., Van Coillie, F., De Wulf, R. 2018. Multi-Date Sentinel1 SAR Image Textures Discriminate Perennial Agroforests in a Tropical Forest-Savannah Transition Landscape. *International Archives of the Photogrammetry, Remote Sensing and Spatial Information Sciences - ISPRS Archives, 42*, 339-346. https://doi.org/10.5194/isprs-archives-XLII-1-339-2018

Numbisi, F.N., Van Coillie, F., De Wulf, R. 2019. Delineation of Cocoa Agroforests Using Multiseason Sentinel-1 SAR Images: A Low Grey Level Range Reduces Uncertainties in GLCM Texture-Based Mapping. *ISPRS International Journal of Geo-Information, 8*(4), 179. https://doi.org/10.3390/ijgi8040179

Numbisi, F.N., Van Coillie, F. 2020. Does Sentinel-1A Backscatter Capture the Spatial Variability in Canopy Gaps of Tropical Agroforests? A Proof-of-Concept in Cocoa Landscapes in Cameroon. *Remote Sensing, 12*(24), 1–29. https://doi.org/10.3390/rs12244163

Nyoungui, A.N., E. Tonye, Akono, A. 2002. Evaluation of Speckle Filtering and Texture Analysis Methods for Land Cover Classification from SAR Images. *International Journal of Remote Sensing, 23*(9), 1895–1925. https://doi.org/10.1080/01431160110036157

Oliver, C., Quegan. S. 2004. Understanding Synthetic Aperture Radar Images. Raleigh: SciTech.

Ozesmi, S.L., Bauer, M.E. 2002. Satellite remote sensing of wetlands. *Wetlands Ecology and Management*, *10*, 381–402. https://doi.org/10.1023/A:1020908432489

Otukei, J.R., Blaschke, T. 2010. Land Cover Change Assessment Using Decision Trees, Support Vector Machines and Maximum Likelihood Classification Algorithms. *International Journal of Applied Earth Observation and Geoinformation*, *12*(1), S27-S31. https://doi.org/10.1016/j.jag.2009.11.002

Pal, M. 2005. Random Forest Classifier for Remote Sensing Classification. *International Journal of Remote Sensing, 26*(1), 217–222. https://doi.org/10.1080/01431160412331269698

Panuju D.R., Paull, D.J., Trisasongko, B.H. 2019. Combining Binary and Post-Classification Change Analysis of Augmented ALOS Backscatter for Identifying Subtle Land Cover Changes. *Remote Sensing, 11*(1), 100. https://doi.org/10.3390/rs11010100

Pedregosa, F., Varoquaux, G., Gramfort, A., Michel, V., Thirion, B., Grisel, O., Blondel, M., Pettenhofer, P., Weiss, R., Dubourg, V., Vanderplas, J., Passos, A., Cournapeau, D., Brucher, M., Perrot, M., Duchescay, E., 2011. Scikit-Learn: Machine Learning in Python. *Journal of Machine Learning Research, 12*, 2850–2830.

Planet Team. 2017. Planet Application Program Interface: In Space for Life on Earth.

Pulella, A., Sica, F., Rizzoli, P. 2020. Monthly Deforestation Monitoring with Sentinel-1 Multi-Temporal Signatures and InSAR Coherences. *Revista de Teledetección,* (56), 1–22. https://doi.org/10.4995/raet.2020.14308

Reid, W., Mooney, H., Cropper, A., Capistrano, D., Carpenter, S., Chopra, K., Dasgupta, P., Dietz, T., Duraiappah, A., Hassan, R., Kasperson, R., Leemans, R., May, R., Mcmichael, A., Pingali, P., Samper, C., Scholes, R., Watson, R., Zakri, A.H., Zurek, M. 2005. *Millenium Ecosystem Assessment Synthesis Report*. https://doi.org/10.1109/IGARSS.2008.4778803

Salvia, M., Grings, F., Karszenbaum, H., Ferrazzoli, P., Kandus, P., Soldano, A., Guerriero, L. 2008. Monitoring Inundation Dynamics in Paraná River, Argentina, by C and L Band SAR. *International Geoscience and Remote Sensing Symposium (IGARSS),* 1, 102-105.

Salvia, M.M., Karszenbaum, H., Kandus, P., Grings, F.M. 2009. Datos Satelitales Ópticos y de Radar Para El Mapeo de Ambientes En Macrosistemas de Humedal. *Revista de Teledetección,* (31), 35–51. Accesible at http://www.aet.org.es/?q=revista31-5

Sivasankar, T., Kumar, D., Srivastava, H.S., Patel, P. 2018. Advances in Radar Remote Sensing of Agricultural Crops: A Review. *International Journal on Advanced Science, Engineering and Information Technology, 8*(4), 1126–1137. https://doi.org/10.18517/ijaseit.8.4.5797

Treitz, P.M., Howarth, P.J., Filho, O.R., Soulis, E.D., 2000. Agricultural Crop Classification Using SAR Tone and Texture Statistics. *Canadian Journal of Remote Sensing, 26*(1), 18–29. https://doi.org/10.1080/07038992.2000.10874751

Tsyganskaya, V., Martinis, S., Marzahn, P, Ludwig, R., 2018. Detection of Temporary Flooded Vegetation Using Sentinel-1 Time Series Data. *Remote Sensing, 10*(8), 1286. https://doi.org/10.3390/rs10081286

Vanama, V.S.K., Mandal, D., Rao., Y.S., 2020. GEE4FLOOD: Rapid Mapping of Flood Areas Using Temporal Sentinel-1 SAR Images with Google Earth Engine Cloud Platform. *Journal of Applied Remote Sensing,* 14(3), 1-23. https://doi.org/10.1117/1.JRS.14.034505